ETH
Eidgenössische Technische Hochschule Zürich
Swiss Federal Institute of Technology Zurich

Seminar for Applied Mathematics SAM

Multi-level Monte Carlo finite volume method for shallow water equations with uncertain parameters applied to landslides-generated tsunamis

C. Sanchez-Linares and M. de la Asunci on and M. Castro and S. Mishra

and J. Šukys

Research Report No. 2014-24
September 2014

Seminar für Angewandte Mathematik
Eidgenössische Technische Hochschule
CH-8092 Zürich
Switzerland

Funding ERC: 306279 SPARCCLE
Funding: Spanish Government Research project MTM2012-38383-C02-01,
Andalusian Government Research project P11-FQM-8179,
and the Swiss Federal Institute of Technology, ETH.

Multi-level Monte Carlo finite volume method for shallow water equations with uncertain parameters applied to landslides-generated tsunamis

C. Sánchez-Linares[1], M. de la Asunción[1], M.J. Castro[1], S. Mishra[2], and J. Šukys[2]

[1]Department of Mathematical Analysis, University of Málaga, Spain
[2]Department of Mathematics, ETH, Zurich, Switzerland

September 10, 2014

Corresponding author's contact information

- Full name: Carlos Sánchez Linares
- Affiliation: Department of Mathematical Analysis, University of Málaga, Spain.
- Phone: +34 952137423
- Fax: +34 952131894
- email: csl@uma.es

Abstract

Two layer Savage-Hutter type shallow water PDEs model flows such as tsunamis generated by rockslides. On account of heterogeneities in the composition of the granular matter, these models contain uncertain parameters like the ratio of densities of layers, Coulomb and interlayer friction. These parameters are modeled statistically and quantifying the resulting solution uncertainty (UQ) is a crucial task in geophysics. We propose a novel paradigm for UQ that combines the recently developed IFCP spatial discretizations with the recently developed Multi-level Monte Carlo (MLMC) statistical sampling method and provides a fast, accurate and computationally efficient framework to compute statistical quantities of interest. Numerical experiments, including realistic simulations of the Lituya Bay mega tsunami, are presented to illustrate the robustness of the proposed UQ algorithm.

Keywords:
finite volume method; shallow water equations; uncertainty quantification; landslides-generated tsunamis

1 Introduction

Many interesting geophysical phenomena are modeled by systems of nonlinear hyperbolic and convection dominated partial differential equations (PDEs) such as the (conservative) shallow water equations, the (non-conservative) two-layer shallow water equations and their variants. Examples include the propagation of tsunamis (generated by earthquakes or by rockslides), storm surges, tidal waves, avalanches and debris flows.

It is well known that solutions of hyperbolic PDEs take the form of waves that propagate at a finite speed. Furthermore, the solutions might form discontinuities such as shocks, hydraulic jumps, shear layers etc, even when the initial data are smooth. Thus, it is customary to interpret the solutions of such nonlinear PDEs in the sense of distributions. There are innate difficulties in defining such weak solutions for systems that are not in the conservation form. For such systems, special theories such as those in [8] have been proposed. Moreover, weak solutions are not necessarily unique and further admissibility criteria such as entropy conditions need to be imposed in order to single out a physically relevant solution.

Various types of numerical methods have been designed to approximate these convection-dominated nonlinear hyperbolic PDEs efficiently. Methods such as finite volume, finite difference and discontinuous Galerkin finite element schemes are widely used. In particular, the approximation of non-conservative systems is quite involved as the right jump conditions across discontinuities need to be approximated [26]. An attractive framework to deal with such problems is the one of path conservative numerical schemes developed by Pares [25].

Numerical methods to approximate these nonlinear hyperbolic PDEs (or for that matter any PDE) require inputs such as the initial data, boundary

conditions and coefficients in the fluxes, sources and viscous (other regularizing) terms of the PDE. These inputs need to be measured. Measurements are marked by uncertainty. For instance, one can think of an earthquake generating a tsunami. In such a situation, the initial conditions are typically estimated from a very uncertain measurement process. This uncertainty in determining the inputs to the PDE is propagated into the solution. The calculation of solution uncertainty, given input uncertainty, falls under the rubric of uncertainty quantification (UQ). UQ for geophysical flows is vitally important for risk evaluation and hazard mitigation.

Although various approaches to modeling input uncertainty exist, the most popular framework models input uncertainty statistically in terms of random parameters and random fields. The resulting PDE is a *stochastic* (random) PDE. The solution has to be sought for in a stochastic sense and statistical quantities such as the mean, the variance, higher moments, confidence intervals and the probability distribution function (pdfs) of the solution are the objects of interest.

The modeling and computation of solution statistics is highly non-trivial. Challenges include possibly large number of random variables (fields) to parametrize the uncertainty and the sheer computational challenge of evaluating statistical moments that might necessitate a large number of PDE solves. The challenges are particularly accentuated for hyperbolic and convection-dominated PDEs as the discontinuities in physical space such as shocks can propagate into stochastic space resulting in a loss of regularity of the underlying solution with respect to the random parameters. A very large number of degrees of freedom in stochastic space might be needed to resolve such irregular functions. See a recent review [1] for a detailed account of the challenges involved in UQ for hyperbolic problems.

Nevertheless, several numerical methods have been developed for UQ in hyperbolic PDEs. See [6, 27, 29, 30, 31, 32]) and the review [1] for details. Methods include the stochastic Galerkin methods based on generalized Polynomial Chaos (gPC), stochastic collocation methods and stochastic finite volume methods (SFVM). Some of these methods (particularly stochastic Galerkin) have the huge disadvantage of being highly intrusive: existing codes for computing deterministic solutions of conservation laws need to be completely reconfigured for implementation. Furthermore, none of these methods are currently able to handle even a moderate number of sources of uncertainty (stochastic dimensions).

Another class of methods are the so-called Monte Carlo (MC) methods in which the probability space is sampled, the underlying deterministic PDE is solved for each sample and the samples are combined to determine statistical information about the random field. Although non-intrusive, easy to code and to parallelize, MC methods converge at rate 1/2 as the number M of MC samples increases. The asymptotic convergence rate $M^{-1/2}$ is non-improvable by the central limit theorem.

Therefore, MC methods require a large number of "samples"(with each "sample" involving the numerical solution of the underlying PDE with a given draw of parameter values) in order to ensure low statistical errors. This slow convergence entails high computational costs for MC type methods and makes

them infeasible for computing uncertainty in complex shallow water flows. We refer to [21] for a detailed error and computational complexity analysis for the MC method in the context of scalar conservation laws. This slow convergence has inspired the development of Multi-Level Monte Carlo or MLMC methods [16, 17, 18]. In particular, [21] and [22] extend and analyze the MLMC algorithm for scalar conservation laws and for systems of conservation laws, respectively. The asymptotic analysis for the MLMC method, presented in [21], showed that the method allows the computation of approximate statistical moments with the same accuracy versus cost ratio as a single deterministic solve on the same mesh.

Although MLMC methods have been successfully employed in compressible fluid dynamics and magnetohydrodynamics, the application of these methods to perform UQ in geophysical flows has been limited to a model case of the shallow water flows modeled by the single layer shallow water equations with uncertain initial data and bottom topography [23]. It is unclear whether these methods will be efficient in performing UQ for realistic geophysical flows. The investigation of this question is one of the core aims of the current article.

Here, we will consider a realistic geophysical scenario of the flow of two superposed immiscible layers in which a layer of fluidized granular matter is assumed to flow within an upper layer of an inviscid fluid (water). This situation is modeled by a two-layer Savage-Hutter type model introduced in [12]. The resulting PDE is a nonlinear non-conservative hyperbolic system with nonlinear source terms and can model diverse geophysical phenomena such as tsunamis that are generated by rockslides. Apart from the initial conditions and the bottom topography, the model is characterized by three crucial parameters, namely the ratio of the densities of the two layers, the interlayer friction parameter and the Coulomb friction angle. All three parameters need to be measured. These measurements are highly uncertain given that most granular materials are highly heterogeneous and need to be modeled statistically. Thus, UQ in the context of this two-layer shallow water model is the task of determining solution statistics such as the mean and variance of run-up heights, given the uncertainty in the layer density ratio, interlayer friction and Coulomb friction angle.

Our main aim in the current paper is to perform an efficient Uncertainty quantification (UQ) for this two-layer Savage-Hutter model and to validate the results with realistic data. To this end, we will

- Discretize the Savage-Hutter equations in space-time using the highly efficient path-conservative IFCP scheme of [13].
- Model the uncertainty in the key parameters such as ratio of the densities of two layers, the Coulomb friction angle and the interlayer friction by random variables.
- Adapt the Multi-level Monte Carlo (MLMC) method of [21, 22, 23] to compute solution statistics efficiently.
- Benchmark the method and results on three test cases of increasing difficulty namely,

– A one-dimensional submarine landslide over a flat bottom topography.

– A one-dimensional laboratory experiment performed by Fritz et. al in [14] to reproduce the massive run-up Lituaya Bay mega-tsunami of 1958.

– The two-dimensional Lituya Bay mega tsunami.

To the best of our knowledge, this is the first UQ calculation for a realistic geophysical flow such as a tsunami generated by a rockslide using the MLMC methods and demonstrates the power of the judicious combination of efficient numerical schemes such as the IFCP schemes and the Multi-level Monte Carlo (MLMC) method in performing realistic large scale UQ simulations.

The rest of the paper is organized as follows: we present the two-layer Savage-Hutter model in section 2 and the path-conservative IFCP scheme to approximate it in section 3. The Monte Carlo and Multi-level Monte Carlo methods are described in sections 4, 5 and numerical results are presented in section 6.

2 The Savage-Hutter model

We consider a simplified one-dimensional version of the Savage-Hutter type model of [12] given by,

$$\begin{cases} \dfrac{\partial h_1}{\partial t} + \dfrac{\partial q_1}{\partial x} = 0 \\ \dfrac{\partial q_1}{\partial t} + \dfrac{\partial}{\partial x}\left(\dfrac{q_1^2}{h_1} + \dfrac{g}{2}h_1^2\right) + gh_1\dfrac{\partial h_2}{\partial x} = gh_1\dfrac{dH}{dx} + S_f + S_{b_1} \\ \dfrac{\partial h_2}{\partial t} + \dfrac{\partial q_2}{\partial x} = 0 \\ \dfrac{\partial q_2}{\partial t} + \dfrac{\partial}{\partial x}\left(\dfrac{q_2^2}{h_2} + \dfrac{g}{2}h_2^2\right) + rgh_2\dfrac{\partial h_1}{\partial x} = gh_2\dfrac{dH}{dx} - rS_f + \tau. \end{cases} \tag{2.1}$$

Here, the indices 1 and 2 refer to the upper layer (water) and the lower layer (granular matter such mud, rock etc), respectively. The fluid is assumed to occupy a straight channel with constant rectangular cross-section and constant width. The coordinate $x \in [a, b]$ refers to the axis of the channel and t is time, and g is the gravity acceleration. $H(x)$ represents the depth function measured from a fixed level of reference. Each layer is assumed to have a constant density, ρ_i, $i = 1, 2$ ($\rho_1 < \rho_2$), and $r = \rho_1/\rho_2$ is the ratio of densities. In order to model partially fluidized avalanches, we consider a grain layer of density ρ_s, and porosity ψ_0. We consider that the pores in the grain layer are filled with the fluid of the upper layer. Then the density of the second layer is defined as

$$\rho_2 = (1 - \psi_0)\rho_s + \psi_0\rho_1. \tag{2.2}$$

The unknowns $q_i(x,t)$ and $h_i(x,t)$ represent the mass-flow and the thickness, respectively, of the i-th layer at the section of coordinate x at time t. The mean velocity at each layer is related to q_i and h_i by $u_i = q_i/h_i$. The parameter τ parametrizes the Coulomb friction term (see [12]). In this model, this term must be interpreted as:

$$\text{if } |\tau| \geq \sigma^c \Rightarrow \tau = -g(1-r)h_2 \frac{q_2}{|q_2|}\tan(\delta_0), \tag{2.3}$$

$$\text{if } |\tau| < \sigma^c \Rightarrow q_2 = 0, \tag{2.4}$$

where $\sigma^c = g(1-r)h_2\tan(\delta_0)$, with $\delta_0 > 0$ is the Coulomb friction angle.

The terms S_f and S_{b_1} parametrize the friction terms between the layers and the bottom topography, respectively. S_{b_1} follows a Manning law, and S_f is defined by a quadratic friction term:

$$S_{b_1} = -gh_1 \frac{n_1^2}{h_1^{4/3}} u_1|u_1|, \qquad S_f = c_f \frac{h_1 h_2}{h_2 + rh_1}(u_2 - u_1)|u_2 - u_1|.$$

We observe that S_{b_1} is imposed to be zero if $h_2 > 0$.

Notice that system (2.1) can be written in the following form:

$$w_t + F(w)_x + B(w)w_x = S(w)H_x + S_F(w), \tag{2.5}$$

where

$$w = \begin{bmatrix} h_1 \\ q_1 \\ h_2 \\ q_2 \end{bmatrix}, \quad F(w) = \begin{bmatrix} q_1 \\ \dfrac{q_1^2}{h_1} + \dfrac{g}{2}h_1^2 \\ q_2 \\ \dfrac{q_2^2}{h_2} + \dfrac{g}{2}h_2^2 \end{bmatrix}, \quad S(w) = \begin{bmatrix} 0 \\ gh_1 \\ 0 \\ gh_2 \end{bmatrix}, \tag{2.6}$$

$$B(w) = \begin{bmatrix} 0 & 0 & 0 & 0 \\ 0 & 0 & gh_1 & 0 \\ 0 & 0 & 0 & 0 \\ grh_2 & 0 & 0 & 0 \end{bmatrix} \quad \text{and} \quad S_F(w) = \begin{bmatrix} 0 \\ S_f + S_{b_1} \\ 0 \\ -rS_f + \tau \end{bmatrix}. \tag{2.8}$$

The vector w takes values in the set:

$$\mathcal{O} = \{[h_1, q_1, h_2, q_2]^T \in \mathbb{R}^4, \quad h_1 \geq 0, h_2 \geq 0\}$$

as the thickness of the layers may vanish in practical applications when one or the two layers disappear in part of the domain.

Adding to (2.5) the equation $H_t = 0$, the system can be written in the form

$$W_t + \mathcal{A}(W)\cdot W_x = \widetilde{S_F}(W) \tag{2.9}$$

where W is the augmented vector

$$W = \begin{bmatrix} w \\ H \end{bmatrix} \in \mathbf{\Omega} = \mathcal{O} \times \mathbb{R},$$

$\mathcal{A}$ is the 5×5 matrix whose block structure is given by:

$$\mathcal{A}(W) = \left[\begin{array}{c|c} A(w) & -S(w) \\ \hline 0 & 0 \end{array}\right]$$

where $A(w) = J(w) + B(w)$, being $J(w) = \dfrac{\partial F}{\partial w}(w)$:

$$A(w) = \begin{bmatrix} 0 & 1 & 0 & 0 \\ -u_1^2 + gh_1 & 2u_1 & gh_1 & 0 \\ 0 & 0 & 0 & 1 \\ rgh_2 & 0 & -u_2^2 + gh_2 & 2u_2 \end{bmatrix}, \tag{2.10}$$

and $\widetilde{S_F}(W)$ is the augmented vector

$$\widetilde{S_F}(W) = \begin{bmatrix} S_F(w) \\ 0 \end{bmatrix}.$$

As mentioned in the introduction, solutions of (2.9) may develop discontinuities and the solution needs to interpreted in the weak sense. However, on account of the non-conservative form of the equations, the usual notion of weak solution in the sense of distributions cannot be used. The theory introduced by Dal Maso, LeFloch, and Murat [8] is followed here to define weak solutions of (2.9). This theory allows one to define the nonconservative product $\mathcal{A}(W) \cdot W_x$ as a bounded measure provided a family of Lipschitz continuous paths $\Phi : [0,1] \times \Omega \times \Omega \to \Omega$ is prescribed, which must satisfy certain natural regularity conditions. Notice that the meaning of the nonconservative products and thus the concept of weak solution has to be assigned together with the system of equations, and its initial/boundary conditions. A detailed description of how paths can be chosen is discussed in [26]. Here, we consider paths defined by the family of straight segments.

Finally, the stationary solutions of interest for the above system are those of water at rest, i.e, $u_1 = u_2 = 0$ are given by:

$$\begin{cases} u_1 = u_2 = 0 \\ h_1 + h_2 - H = \text{constant} \\ \partial_x(h_2 - H) < \tan(\delta_0), \end{cases} \tag{2.11}$$

and, in particular,

$$\begin{cases} u_1 = u_2 = 0 \\ h_1 + h_2 - H = \text{constant} \\ h_2 - H = \text{constant} \end{cases} \tag{2.12}$$

are solutions of system (2.1).

3 The IFCP numerical scheme

We discretize system (2.1) by dividing the 1D-domain $D = [a, b]$ into L cells or finite volumes $I_i = [x_{i-1/2}, x_{i+1/2}]$, where Δx is the length of each cell which, for simplicity, is assumed to be constant. Let us denote by $\mathcal{T}$ the partition of the domain D by the cells I_i. We denote by w_i^n and approximation of the average of the solution at the i-th cell at time $t^n = n\Delta t$

$$w_i^n \cong \frac{1}{\Delta x} \int_{x_{i-1/2}}^{x_{i+1/2}} w(x, t^n)\, dx.$$

To begin with, we describe the first order numerical scheme that we use: it is a three-step method, where in the first step, we neglect the friction terms and the path-conservative IFCP scheme (see [13]) is used. Then, in the other two steps, the friction terms will be discretized in a semi-implicit manner. We denote the three steps as follows:

$$w_i^n \to w_i^{n+1/3} \to w_i^{n+2/3} \to w_i^{n+1}.$$

The result of the first step, $w_i^{n+1/3}$, is computed using the IFCP scheme, as follows:

$$w_i^{n+1/3} = w_i^n - \frac{\Delta t}{\Delta x}\left(D_{i-1/2}^{\tau,+}(w_{i-1}^n, w_i^n, H_{i-1}, H_i) + D_{i+1/2}^{\tau,-}(w_i^n, w_{i+1}^n, H_i, H_{i+1})\right) \tag{3.1}$$

where $D_{i+1/2}^{\tau,\pm}(w_i^n, w_{i+1}^n, H_i, H_{i+1})$ are fluctuations in a modified IFCP scheme that takes into account the presence of the Coulomb friction term (see [12, 13]) and are defined as follows:

$$\begin{aligned} D_{i+1/2}^{\tau,-} &= \frac{1}{2}\Big(R_{i+1/2} - \big(\alpha_{0,i+1/2}\widetilde{I}_{i+1/2}^{\tau} + \alpha_{1,i+1/2}R_{i+1/2}^{\tau} + \alpha_{2,i+1/2}A_{i+1/2}R_{i+1/2}^{\tau}\big)\Big) \\ &\quad + F_Q(w_i), \\ D_{i+1/2}^{\tau,+} &= \frac{1}{2}\Big(R_{i+1/2} + \big(\alpha_{0,i+1/2}\widetilde{I}_{i+1/2}^{\tau} + \alpha_{1,i+1/2}R_{i+1/2}^{\tau} + \alpha_{2,i+1/2}A_{i+1/2}R_{i+1/2}^{\tau}\big)\Big) \\ &\quad - F_Q(w_{i+1}), \end{aligned} \tag{3.2}$$

where the coefficients $\alpha_{k,i+1/2}$, $k = 0, 1, 2$ are defined in terms of the eigenvalues of the 1D two-layer shallow-water system following [13].

The matrix $A_{i+1/2}$ is defined by

$$A_{i+1/2} = \begin{pmatrix} 0 & 1 & 0 & 0 \\ gh_{1,i+1/2} - \big(u_{1,i+1/2}\big)^2 & 2u_{1,i+1/2} & gh_{1,i+1/2} & 0 \\ 0 & 0 & 0 & 1 \\ rgh_{2,i+1/2} & 0 & gh_{2,i+1/2} - \big(u_{2,i+1/2}\big)^2 & 2u_{2,i+1/2} \end{pmatrix} \tag{3.3}$$

with

$$u_{k,i+1/2} = \frac{\sqrt{h_{k,i}}\, u_{k,i} + \sqrt{h_{k,i+1}}\, u_{k,i+1}}{\sqrt{h_{k,i}} + \sqrt{h_{k,i+1}}}\ ,$$

and

$$h_{k,i+1/2} = \frac{h_{k,i} + h_{k,i+1}}{2}, \quad k = 1, 2.$$

$F_Q(w)$ is given by

$$F_Q(w) = \begin{pmatrix} q_1 & \frac{q_1^2}{h_1} & q_2 & \frac{q_2^2}{h_2} \end{pmatrix}^T.$$

$\widetilde{I}^{\tau}_{i+1/2}$ is defined by

$$\widetilde{I}^{\tau}_{i+1/2} = \begin{cases} \widetilde{I}_{i+1/2} & \text{if } |h_{2,i+1/2}\, u_{2,i+1/2}| > \Delta t\, \sigma^c_{i+1/2} \\ \begin{pmatrix} \mu_{1,i+1} - \mu_{1,i} \\ q_{1,i+1} - q_{1,i} \\ 0 \\ q_{2,i+1} - q_{2,i} \end{pmatrix} = \begin{pmatrix} \Delta_{i+1/2}\mu_1 \\ \Delta_{i+1/2} q_1 \\ 0 \\ \Delta_{i+1/2} q_2 \end{pmatrix} & \text{otherwise} \end{cases}$$

with $\sigma^c_{i+1/2} = g(1-r)h_{2,i+1/2}\tan(\delta_0)$ and

$$\widetilde{I}_{i+1/2} = \begin{pmatrix} \Delta_{i+1/2}\mu_1 - \Delta_{i+1/2}\mu_2 & \Delta_{i+1/2} q_1 & \Delta_{i+1/2}\mu_2 & \Delta_{i+1/2} q_2 \end{pmatrix}^T$$

where $\mu_{k,i}$, $k = 1, 2$ $\mu_{1,i} = h_{1,i} + h_{2,i} - H_i$ and $\mu_{2,i} = h_{2,i} - H_i$.

$R^{\tau}_{i+1/2}$ is defined by:

$$R^{\tau}_{i+1/2} = \begin{cases} R_{i+1/2} & \text{if } |h_{2,i+1/2}\, u_{2,i+1/2}| > \Delta t\, \sigma^c_{i+1/2} \\ F_Q(w_{i+1}) - F_Q(w_i) + P^{\tau}_{i+1/2} & \text{otherwise} \end{cases}$$

where $R_{i+1/2}$ is defined by

$$R_{i+1/2} = F_Q(w_{i+1}) - F_Q(w_i) + P_{i+1/2},$$

with

$$P_{i+1/2} = \begin{pmatrix} 0 & g h_{1,i+1/2}\Delta_{i+1/2}\mu_1 & 0 & g h_{2,i+1/2}\big(r\Delta_{i+1/2}\mu_1 + (1-r)\Delta_{i+1/2}\mu_2\big) \end{pmatrix}^T$$

and finally,

$$P^{\tau}_{i+1/2} = \begin{pmatrix} 0 & g h_{1,i+1/2}\Delta_{i+1/2}\mu_1 & 0 & r g h_{2,i+1/2}\Delta_{i+1/2}\mu_1 \end{pmatrix}^T.$$

The resulting numerical scheme is explicit, therefore, it is necessary to impose a CFL (Courant-Friedrichs-Lewy) condition to ensure linear stability of the scheme. In practice, this condition implies a restriction on the time step given by:

$$\Delta t^n = \min_i \gamma \frac{\Delta x}{\max |\lambda_{i+1/2}|} \tag{3.4}$$

where $0 < \gamma \leq 1$ and $\lambda_{i+1/2}$ are the eigenvalues of matrix $A_{i+1/2}$.

Finally, we use the modification of the numerical scheme proposed in [3] in order to deal with wet-dry transitions.

3.0.1 Second step: computation of $w_i^{n+2/3}$

Once $w_i^{n+1/3}$ has been computed, we define $w_i^{n+2/3}$ as:

$$w_i^{n+2/3} = \begin{pmatrix} h_{1,i}^{n+1/3} & q_{1,i}^{n+2/3} & h_{2,i}^{n+1/3} & q_{2,i}^{n+2/3} \end{pmatrix}^T \tag{3.5}$$

with $q_{k,i}^{n+2/3} = u_{k,i}^{n+2/3} h_{k,i}^{n+1/3}$, $k = 1, 2$, where $u_{k,i}^{n+2/3}$, $k = 1, 2$, is the solution of the linear system:

$$\begin{cases} u_{1,i}^{n+2/3} = u_{1,i}^{n+1/3} + a\, h_{2,i}^{n+1/3} \left(u_{2,i}^{n+2/3} - u_{1,i}^{n+2/3} \right) - \dfrac{\Delta t\, g\, n_1^2}{\left(h_{1,i}^{n+1/3} \right)^{4/3}} \left| u_{1,i}^n \right| u_{1,i}^{n+2/3} \\ u_{2,i}^{n+2/3} = u_{2,i}^{n+1/3} - r\, a\, h_{1,i}^{n+1/3} \left(u_{2,i}^{n+2/3} - u_{1,i}^{n+2/3} \right) \end{cases} \tag{3.6}$$

where

$$a = \Delta t \, \frac{c_f}{r h_{1,i}^{n+1/3} + h_{2,i}^{n+1/3}} \left| u_{1,i}^n - u_{2,i}^n \right|.$$

Note that (3.6) corresponds to a semi-implicit discretization of the friction terms $S_f(w)$ and $S_{b_1}(w)$.

3.0.2 Third step: computation of w_i^{n+1}

Finally, once $w_i^{n+2/3}$ has been determined, we compute w_i^{n+1} by

$$w_i^{n+1} = \begin{pmatrix} h_{1,i}^{n+2/3} & q_{1,i}^{n+2/3} & h_{2,i}^{n+2/3} & q_{2,i}^{n+1} \end{pmatrix}^T \tag{3.7}$$

where

$$q_{2,i}^{n+1} = \begin{cases} \dfrac{|\, q_{2,i}^{n+2/3}\, | q_{2,i}^{n+2/3}}{|\, q_{2,i}^{n+2/3}\, | + \sigma_i\, \Delta t} & \text{if } |q_{2,i}^{n+2/3}\,| \geq \sigma_i\, \Delta t \\ 0 & \text{otherwise} \end{cases}$$

with $\sigma_i = g(1-r) h_{2,i}^{n+2/3} \tan(\delta_0)$.

The resulting scheme is exactly well-balanced for water at rest solutions ($u_1 = u_2 = 0$ and μ_1 and μ_2 constant). Moreover, the scheme is able to approximate accurately the stationary solutions corresponding to $u_1 = u_2 = 0$, μ_1 constant and $\partial_x \mu_2 < \tan(\delta_0)$, i.e, a stationary water at rest solution for which the Coulomb friction term balances the pressure term in the granular material (see [12]).

Second order approximations is obtained following the procedure described in [5], using MUSCL reconstruction of the unknowns μ_1, q_1, μ_2, q_2 and H together with the second order TVD Runge-Kutta method.

4 Monte Carlo method

4.1 Modeling uncertain inputs

As mentioned in the introduction, it is not possible to measure precisely some of the parameters present in system (2.1). This is the case of the parameters related to friction terms or the ratio of densities in a non-homogeneous media. Here, we consider the term involved in friction between the two layers, c_f, the ratio between densities, r, and the Coulomb friction angle, denoted by δ_0.

Uncertainty in input values for these parameters leads to uncertainty in the solution w of the system (2.5). Therefore, noting by $(\Omega, F, \mathbb{P})$ the complete probability space, $w(t, x, \xi)$, $\xi \in \Omega$ is the solution of the system

$$w_t(\xi) + F(w)_x + B(w, \xi)w_x = S(w)H_x + S_F(w, \xi). \tag{4.1}$$

4.2 Monte Carlo finite volume method

In order to approximate the random system of equations (4.1), we need to discretize the probability space. The simplest sampling method is the Monte Carlo (MC) algorithm that consists of the following steps:

1. **Sample:** We draw M independent identically distributed (i.i.d) samples of c_f^k, r^k and δ_0^k with $k = 1, 2, \ldots, M$ from the random fields $c_f(\xi)$, $r(\xi)$ and $\delta_0(\xi)$.

2. **Solve:** For each realization c_f^k, r^k and δ_0^k the underlying system (2.5) is solved by the IFCP-FV method described previously. Let the finite volume solutions be denoted by $w_{\mathcal{T}}^{k,n}$, i.e. by cell averages $\{w_i^{k,n} : I_i \in \mathcal{T}\}$ at time level t^n,

$$w_{\mathcal{T}}^{k,n}(x) = w_i^{k,n}, \quad \forall x \in I_i, I_i \in \mathcal{T}$$

3. **Estimate Statistics:** We estimate the expectation of the random solution field with the sample mean (ensemble average) of the approximate solution:

$$E_M[w_{\mathcal{T}}^n] := \frac{1}{M} \sum_{k=1}^{M} w_{\mathcal{T}}^{k,n}. \tag{4.2}$$

   Higher statistical moments can be approximated analogously. (See [21])

The above algorithm is quite simple to implement. We remark that step 1 requires a (pseudo) random number generator (PRNG). In this work we will use the Mersenne Twister PRNG [19], which has a period of $2^{19937} - 1$. In step 2, an existing code for finite volume methods can be used. For instance, we will use the IFCP scheme presented in the previous section. Furthermore, the only (data) interaction between different samples is in step 3 when ensemble averages are computed. Thus, the MC is non-intrusive as well as easily parallelizable.

Although a rigorous error estimate for the MC approximating the two-layer Savage-Hutter system is currently out of reach, we rely on the analysis for a scalar conservation law (see [21]) and on the numerical experience with the MLMC-FV solution of non-linear hyperbolic systems of conservation laws with random initial data (see [22]) to *postulate* that the following estimate holds:

$$\|\mathbb{E}[w(\cdot,t^n)] - E_M[w_{\mathcal{T}}^n]\|_{L^2(\Omega;L^1(D))} \leq C_{\text{stat}} M^{-1/2} + C_{st}\Delta x^s. \tag{4.3}$$

Here, the $L^2(\Omega;L^1(D))$-norm of the random function $f(\cdot,\xi)$ is defined as

$$\|f\|_{L^2(\Omega;L^1(D))} := \left(\int_{w\in\Omega} \|f(\cdot,\xi)\|^2_{L^1(D)}\, d\mathbb{P}(\xi)\right)^{\frac{1}{2}},$$

and C_{stat}, C_{st} are constants that depend on the domain D, initial condition, topography, time horizon T and the statistics of random parameters $c_f(\xi)$, $r(\xi)$ and $\delta_0(\xi)$, in particular, on mean and variance. In the above, we have assumed that the underlying finite volume scheme converges to the solutions of the deterministic system (2.1) at a rate of $s > 0$. Moreover, in (4.3) and throughout the following, we adopted the (customary in the analysis of MC methods) convention to interpret the MC samples $w_{\mathcal{T}}^{k,n}$ in (4.2) as i.i.d. random functions, with the same law as w. Note that the error estimate for the mean requires that the solution has finite second moments. Based on the error analysis of [21], we need to choose

$$M = \mathcal{O}(\Delta x^{-2s}) \tag{4.4}$$

in order to equilibrate the statistical error with the spatio-temporal error in (4.3).

Consequently, it is straightforward to deduce that the asymptotic error vs. (computational) work estimate is given by (see [21])

$$\|\mathbb{E}[w(\cdot,t^n)] - E_M[w_{\mathcal{T}}^n]\|_{L^2(\Omega;L^1(\mathbb{R}^d))} \lesssim (\text{Work})^{-s/(d+1+2s)}$$

where d is the space dimension (in this paper $d = 1$ or $d = 2$). The above error vs. work estimate is considerably more expensive when compared to the deterministic FVM error which scales as $(\text{Work})^{-s/d+1}$. We see in the situation of low order s of convergence and space dimension, a considerably reduced rate of convergence of the MC-FVM, in terms of accuaracy vs. work, is obtained. On the other hand, for high order schemes (i.e. $s >> d+1$) the MC error dominates and we obtain the rate $1/2$ in terms of work which is typical of MC methods.

5 Multi Level Monte Carlo Finite Volume Method

Given the slow convergence of MC-FV, [21] and [22] proposed the Multi-Level Monte Carlo finite volume method (MLMC-FV). The key idea behind MLMC-FV is to simultaneously draw MC samples on a hierarchy of nested grids.

The algorithm consists of the following four steps:

1. **Nested meshes:** Consider nested meshes $\{\mathcal{T}_l\}_{l=0}^{\infty}$ of the spatial domain D with corresponding mesh diameters Δx_l that satisfy:

$$\Delta x_l = \sup\{\text{diam}(\mathcal{I}) \ : \ \mathcal{I} \in \mathcal{T}_l\} = \mathcal{O}(2^{-l}\Delta x_0), \quad l \in \mathbb{N}_0$$

where Δx_0 is the mesh width for the coarsest resolution and corresponds to the lowest level $l = 0$.

2. **Sampling:** For each level of resolution $l \in \mathbb{N}_0$, we draw M_l independent identically distributed (i.i.d) samples of ${c_f}_l^k$, r_l^k and ${\delta_0}_l^k$, with $k = 1, 2, \ldots, M_l$ belonging to the set of admissible parameters for the model.

3. **Solving:** For each resolution level l and each realization ${c_f}_l^k$, r_l^k and ${\delta_0}_l^k$, the underlying system (4.1) is solved by the IFCP method using mesh $\mathcal{T}_l$. Let the finite volume solutions be denoted by $w_{\mathcal{T}_l}^{k,n}$ for the mesh $\mathcal{T}_l$ and at the time level t_n.

4. **Estimate Solution Statistics:** Fix some positive integer $L < \infty$ corresponding to the highest level. We estimate the expectation of the random solution field with the following estimator:

$$E^L[w(\cdot, t^n)] := E_{M_0}[w_{\mathcal{T}_0}^n] + \sum_{l=1}^{L} E_{M_l}[w_{\mathcal{T}_l}^n - w_{\mathcal{T}_{l-1}}^n], \tag{5.1}$$

with E_{M_l} being the MC estimator

$$E_{M_l}[w_{\mathcal{T}}^n] := \frac{1}{M_l}\sum_{k=1}^{M_l} w_{\mathcal{T}}^{k,n} \tag{5.2}$$

for the level l. Higher statistical moments can be approximated analogously. (See [21]).

MLMC-FV is non-intrusive as any standard FVM code can be used in step 3. Furthermore, MLMC-FV is amenable to efficient parallelization as data from different grid resolutions and different samples only interacts in step 4.

Following the rigorous estimate for error in [21, 22], we consider

$$\|\mathbb{E}[w(\cdot, t^n)] - E^L[w_{\mathcal{T}}^n]\|_{L^2(\Omega;L^1(\mathbb{R}))} \leq C_1\Delta x_L^s + C_2\left\{\sum_{l=0}^{L} M_l^{-1/2}\Delta x_l^s\right\} + C_3 M_0^{-1/2} \tag{5.3}$$

Here s again refers to the convergence rate of the deterministic finite volume scheme and $C_{1,2,3}$ are constants depending only on the initial data, the parameters and the source term. From the error estimate (5.3), we obtain that the number of samples to equilibrate the statistical and spatio-temporal discretization errors in (5.1) is given by

$$M_l = \mathcal{O}(2^{2(L-l)s})$$

Notice that the choice of M_l implies that the largest number of MC samples is required on the coarsest mesh level $l = 0$, whereas only a small fixed number of MC samples are needed on the finest discretization levels.

The corresponding error vs. work estimate for MLMC-FV is given by (see [21, 22])

$$\|\mathbb{E}[w(\cdot, t^n)] - E^L[w_{\mathcal{T}}^n]\|_{L^2(\Omega;L^1(\mathbb{R}))} \lesssim (\text{Work})^{-s/(d+1)} \cdot \log(\text{Work}), \tag{5.4}$$

provided $s < (d+1)/2$. The above estimate shows that MLMC-FV is more efficient than MC-FV. Also, MLMC-FV is (asymptotically) of the same complexity as a single deterministic FVM solve.

6 Numerical experiments

6.1 Submarine landslide over a flat bottom topography

As a first numerical experiment, we consider the computational domain $x \in [-5, 5]$ with transparent boundary conditions at both boundaries, and a flat bottom topography, specified by $H(x) \equiv 2$. The initial data for the problem is

$$h_1(x, 0) = \begin{cases} 2 & \text{if } |x| \geq 1 \\ 0.5 & \text{if } |x| < 1 \end{cases},$$

$$h_2(x, 0) = \begin{cases} 0.5 & \text{if } |x| \geq 1 \\ 1.5 & \text{if } |x| < 1 \end{cases},$$

and

$$u_1(x, 0) = 0, \qquad u_2(x, 0) = 0.$$

Hence, our aim is to simulate a submarine landslide as the fluidized granular matter (rock), denoted by the index 2 will slide under the water surface (denoted by index 1) and will initiate a flow of the free surface.

As mentioned in the introduction, the key parameters, that of ratio of the densities of two layers r, the Coulomb angle δ_0 and the interlayer friction parameter c_f are uncertain. Here, we assume that these parameters are random variables that take values from a uniform distribution with following mean values,

$$c_f = 0.0001, \quad r = 0.5, \quad \delta_0 = 35^\circ.$$

Furthermore the variation is assumed to 40% over the mean for each of the three uniformly distributed uncertain parameters. Such a variability is fairly representative of the variability in experiments and observations.

We will perform UQ for the two-layer Savage-Hutter system with the above uncertain inputs using both the first- and second-order IFCP schemes described in section 3 to discrete space-time and both the Monte Carlo (MC) as well as Multi-level Monte Carlo methods, described in sections 4 and 5, respectively, to discretize the probability space.

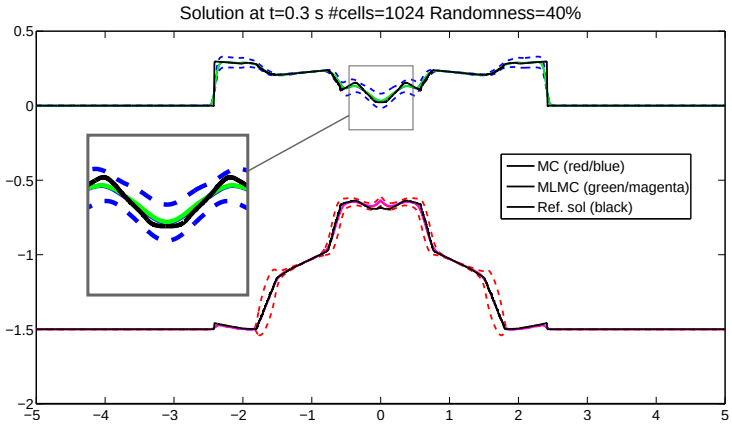

FIGURE 1: First order MC-IFCP & MLMC-IFCP methods for the submarine landslide. The mean and standard deviation of the layer heights at $t = 0.3$ are shown.

The resulting mean and mean $\pm$ standard deviation (statistical spread) are presented in figures 1 and 2. In figure 1, we present statistics of the heights of both layers at time $T = 0.3$ using a first-order IFCP scheme (IFCP1) on a fine mesh of 1024 cells. The scheme is combined with a MC simulation with $M = 1024$ samples. Such a choice of sample number is based on the fact that the MC sample number should be chosen by the formula $M = (\Delta x)^{-2s}$ in (4.4). This reduces to reduces to $M = N$, with N being the number of cells in the current simulation as the convergence rate is $s = 1/2$ for a first-order IFCP scheme. Similarly, the MLMC method (together with the first-order IFCP scheme) is based on choosing $L = 6$ levels of mesh resolution, ranging from $N_0 = 32$ cells up to $N_5 = 1024$ cells. We choose $M_5 = 16$ samples for the highest level of resolution.

The statistics for the height of both layers simulated with the second-order version of the IFCP (IFCP2) scheme, together with MC and MLMC discretizations of the probability space are presented in figure 2. Again, we choose a fine mesh resolution of 1024 cells. $M = 512$ samples are used for the MC-IFCP2 method. As in the first-order case, $L = 6$ levels of mesh resolution are used to specify the MLMC-IFCP2 method, ranging from $N_0 = 32$ cells up to $N_5 = 1024$ cells. We choose $M_5 = 16$ samples for the highest level of resolution.

The solution presented in figures 1 and 2 is fairly complicated and consists of fast moving outer shock waves in both layers, followed by train of slow moving shocks and rarefactions in each layer. It is interesting to note how the non-linear evolution equation (2.1) distributes the uniform uncertainty in the three parameters of interest. As shown in figures 1 and 2, the level of uncertainty in

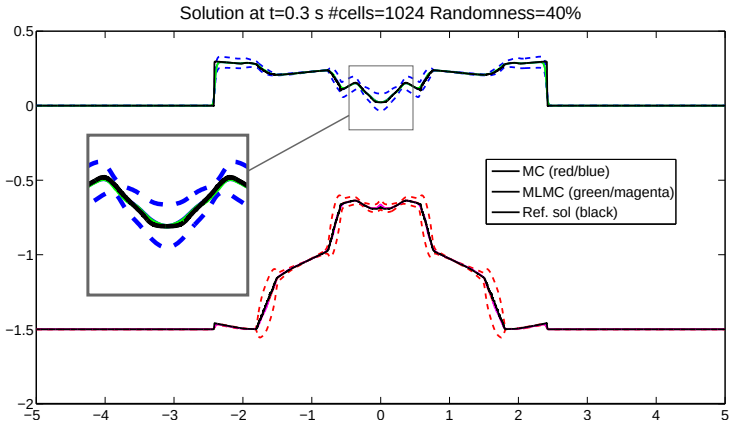

FIGURE 2: Second order MC-IFCP & MLMC-IFCP methods for the submarine landslide. The mean and standard deviation of the layer heights at $t = 0.3$ are shown.

the location as well as amplitude of the fast outer shock waves is rather low. This is not surprising as these waves depend on the total water depth (which is determined exactly initially). On the other hand, the inner slow waves contain a significant amount of uncertainty in both their location (speed) as well as amplitude. It is not possible to resolve this complex distribution of uncertainty by any explicit formulae, given the inherently nonlinear nature of the governing equations. However, our judicious combination of MC-IFCP as well as MLMC-IFCP methods is able to accurately quantify uncertainty.

Comparing the sets of methods, we observe that the second-order IFCP methods resolve the waves more sharply even though the first-order method is quite competitive. Furthermore, the MC and MLMC methods are fairly comparable at the same mesh resolution. In order to compare the methods quantitatively, we compute a reference solution on a fine mesh and with a large number of samples, and plot the error vs. resolution as well as error vs. runtime for both the mean and the variance of the outer layer height h_1 and display the results in figure 3. Note that the statistical errors are estimated by a procedure, first introduced in [21]. As shown in this figure, the second-order IFCP method is superior in the amplitude of the error (for both mean and variance) than the first-order method, when combined with both the MC and MLMC discretization of the probability space. On the other hand, the MC and MLMC methods (either combined with the first-order or the second-order IFCP scheme) are very similar when it comes to the amplitude of the error for the same mesh resolution. The main difference between the methods is discovered when the computational efficiency, measured in terms of error vs. run-time, is compared.

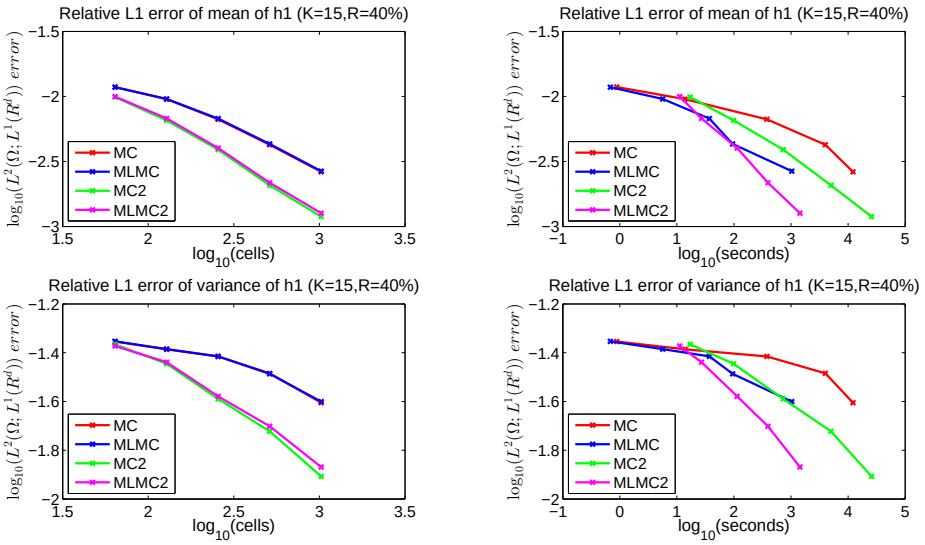

FIGURE 3: Convergence of estimated mean and variance of h_1 in the submarine landslide at $t = 0.3$. First and second order comparison of MC-FV-IFCP and MLMC-FV-IFCP methods.

As seen in figure 3 (right column), the MLMC methods are approximately 60 to 80 times faster than the corresponding MC methods, for the same level of error. This almost two orders of magnitude gain in efficiency with the MLMC methods is instrumental in their utility for performing more realistic UQ simulations at an acceptable computational cost. We consider two such examples below.

6.2 The Lituya Bay mega tsunami

On July 10, 1958, an 8.3 magnitude (on the Richter scale) earthquake, along the Fairweather fault, triggered a major subaerial landslide into the Gilbert Inlet at the head of Lituya Bay on the southern coast of Alaska. The landslide impacted the water at a very high speed generating a giant tsunami with the highest wave runup in recorded history. The mega-tsunami runup was upto an elevation of 524 m and caused total destruction of the forest as well as erosion down to the bedrock on a spur ridge, along the slide axis. Many attempts have been made to understand and simulate this mega tsunami.

6.2.1 A laboratory scale model of Fritz et. al [14]

Based on generalized Froude similarity, Fritz and coworkers constructed a cross section of Gilbert inlet at 1:675 scale in a two-dimensional physical laboratory model ($L \times W \times H$: 11m, 0.5m and 1m), in order to reproduce the run-up heights of the Lituya Bay mega tsunami.

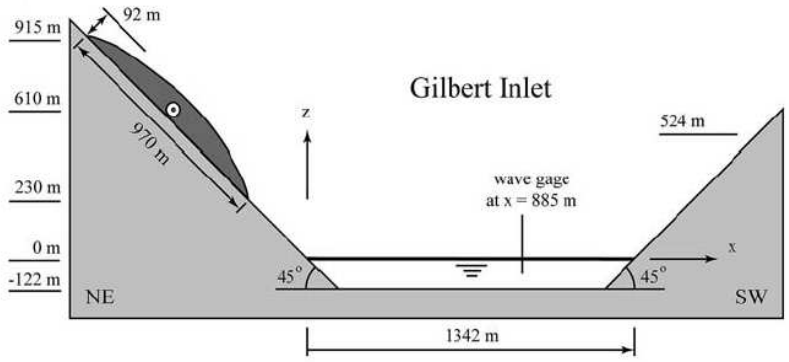

FIGURE 4: Physical model. Cross section of Gilbert Inlet along slide axis in NE to SW orientation

physical parameter	symbol	dimension	value
stillwater depth	h	$[m]$	122
slide thickness	s	$[m]$	92
averaged slide width	b	$[m]$	823
landslide impact velocity	V_s	$[m/s]$	110
slope angle	α	$[\circ]$	45

TABLE 1: Physical considerations for the problem.

In order to reproduce the main features of the slide impact, Fritz and collaborators designed a pneumatic landslide generator. As they intended to model the transition from rigid to granular slide motion, initially, they impulsed the granular material until the landslide achieves a velocity of 110 m/s. This velocity is the approximate impact velocity between the slide and the water surface estimated by Fritz et al., assuming free fall equations for the centroid of the slide. From this instant, the slide is supposed to behave as a granular medium.

In this section, we reproduce numerically the same laboratory experiment: assuming that 110 m/s is a good approximation for the impact velocity of the slide, an initial velocity for the granular layer has been estimated so that the computed impact velocity is approximately 110 m/s. Corresponding to the Fritz's laboratory model (see Figure 4), we consider the following parameters for our simulations, based on the data provided by Fritz experiment. (See Table 1):

The horizontal bottom topography $H(x)$, and initial condition are given by:

$$H(x) = \begin{cases} x + 22 & \text{if } x \in [-1000, 100], \\ 122 & \text{if } x \in (100, 1198), \\ -x + 1320 & \text{if } x \geq 1198, \end{cases} \tag{6.1}$$

$$h_1(x, 0) = \begin{cases} H(x) & \text{if } H(x) \geq 0, \\ 0 & \text{otherwise,} \end{cases} \tag{6.2}$$

$$h_2(x, 0) = \begin{cases} 113 & \text{if } |x + 400| < 265, \\ 0 & \text{otherwise,} \end{cases} \tag{6.3}$$

and

$$u_1(x, 0) = 0, \qquad u_2(x, 0) = 110.$$

As in the previous numerical experiment, we assume that the three crucial uncertain parameters take values from a uniform distribution with following mean values,

$$c_f = 0.0001, \quad r = 0.5, \quad \delta_0 = 35^\circ.$$

Furthermore the variation is assumed to 40% over the mean for each of the three uniformly distributed uncertain parameters.

Motivated by the fact that the second-order IFCP-MLMC method was the most efficient computational technique in the first numerical experiment (it was around two orders of magnitude faster than other methods for the same level of error in mean and variance, see figure 3), we will simulate the 1-D laboratory scale model of Fritz et. al [14] using the second-order IFCP-MLMC method. This method is used with 5 levels of mesh resolution, ranging from $N_0 = 64$ to $N_0 = 1024$ mesh points. The number of samples at the finest level is set as $M_4 = 16$.

The main quantity of interest for the experiment as well as the computation is the run-up height, recorded on a headland ramp. The experimental data for the rune-up height, reported in Fritz el. al [14] is without error bars (statistical spread). We compare it with the results of the second-order IFCP-MLMC simulations in figure 5. Bot the mean run-up height as well as the risk region (statistical spread) are shown in figure 5. The results show excellent qualitative agreement between experiment and simulation. In particular, the maximum run-up height as well as its arrival time are almost exactly matching the experimental data and certainly the experimental data for the maximal run-up height lies within the statistical spread of the simulation. Furthermore, the simulation also shows a second run-up caused by reflections of the first incident wave with the inlet geometry. However, there are quantitative differences, particularly with respect to the arrival time of the reflected wave. This could be very well be on account of modeling error (deficiencies of the two-layer Savage-Hutter model (2.1)) or experimental error (as error bars for the experiment are not available). Furthermore, the simulation clearly identifies possible sensitivity windows. In particular, the uncertainty of the second reflected run-up as well as the build-up to it is identified by the UQ calculation. This is exactly the time

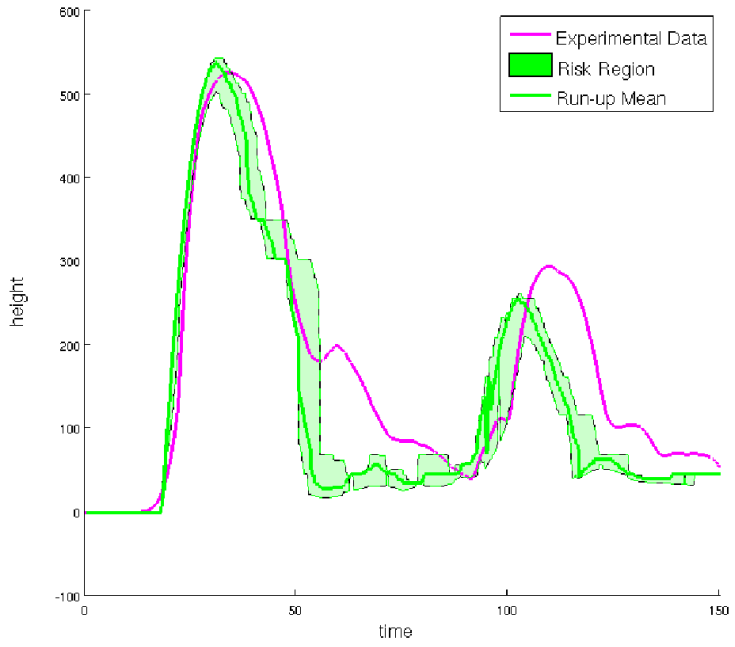

FIGURE 5: Tsunami runup record on headland ramp (magenta) (in the laboratory scale model of Fritz et. al, [14]) vs numerical results (green). Mean & standard deviation. Second order MLMC-FV-IFCP.

window where the difference between the experimental results and the simulation is highest, indicating the possible sensitivity of the experimental results in this time period, with respect to the uncertain parameters.

6.2.2 2D Lituya Bay mega-tsunami

The aim of this section is to produce a realistic, detailed and accurate simulation of the Lituya Bay mega tsunami of 1958, while taking into account uncertainties in critical parameters such as ratios of layer densities, interlayer friction and Coulomb friction. We use public domain topo-bathymetric data as well as the review paper [20] to approximate the Gilbert inlet topo-bathymetry..

Since the underlying domain is two-dimensional, we consider the two-dimensional version of the two-layer Savage-Hutter model (2.1) as presented in [12] and approximate it using a two-dimensional extension of the IFCP scheme. For simplicity, we use the first-order IFCP scheme. For fast computations, this scheme has been implemented on GPUs using the CUDA. This two-dimensional scheme and its GPU adaptation and implementation using single numerical precision are described in detail in [11]. The MLMC-FV-IFCP implementation has also been developed in CUDA, where all the updates of the means and variances

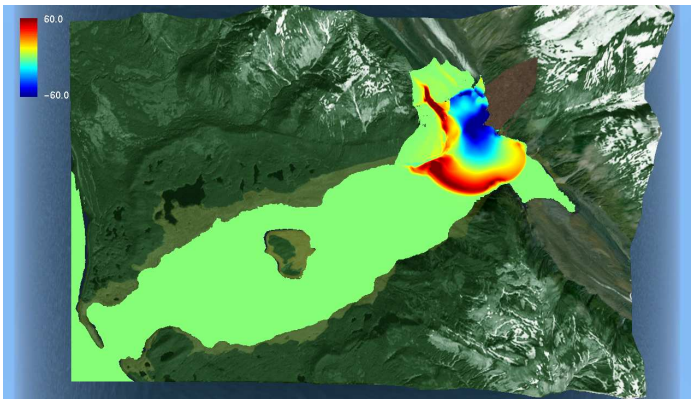

FIGURE 6: Mean of the solution at $t = 39$ s.

FIGURE 7: Variance of the solution at $t = 39$ s.

have also been implemented using CUDA kernels.

A rectangular grid of $3{,}648 \times 1{,}264 = 4{,}611{,}072$ cells with a resolution of $4\,\mathrm{m} \times 7.5\,\mathrm{m}$ has been designed in order to perform this simulation. We compute with the first order MLMC-FV-IFCP method with $L = 4$ levels of resolution and $M_4 = 16$ samples for the highest level, which corresponds to the grid of 4,611,072 cells and constitutes the finest mesh. We allow a 30 % of variability in the parameters c_f, r and δ_0. The mean values of these parameters are $c_f = 0.08$, $r = 0.44$ and $\delta_0 = 13°$. The CFL number is 0.9. Figures 6-9 show the mean solution and variance for 39 s. and 120 s.

The maximum runup is reached at 39 s. We can see in Figures 6 and 7 that the southern propagating part of the initial wave reaches a maximum mean height of 50-60 m. with a maximum standard deviation of 4-5m.

While the initial wave moves through the main axis of Lituya Bay, a larger second wave appears as reflection of the first one from the south shoreline. (see Figures 8 and 9). Both these waves sweep both sides of the shoreline in their

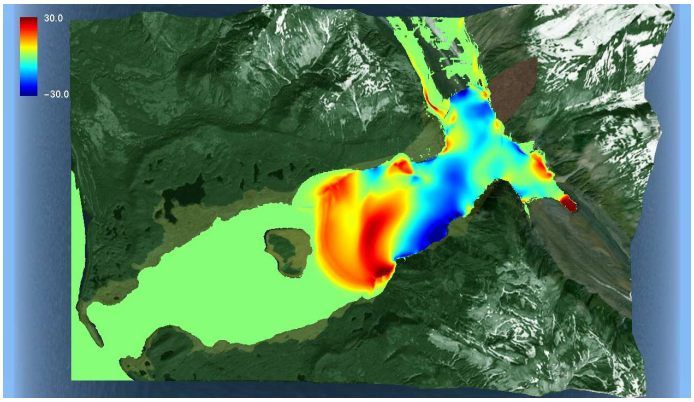

FIGURE 8: Mean of the solution at $t = 120$ s.

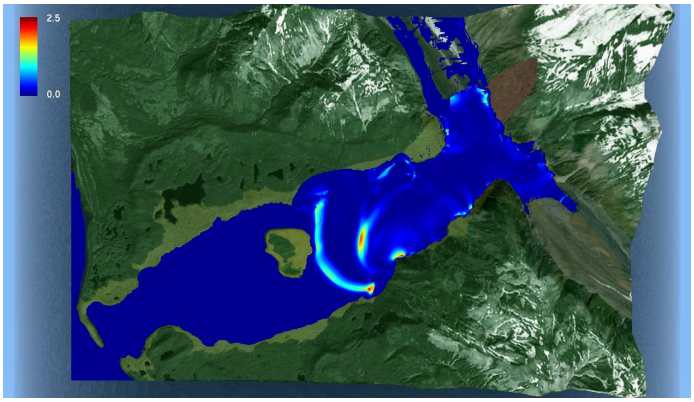

FIGURE 9: Variance of the solution at $t = 120$ s.

path. In the north shoreline, the wave reaches between 15-20 m height while in the south shoreline the wave reaches mean values between 20-30 m assuming a standard deviation of 1.2-1.5 m height.

The impact times, trimlines and the mean and variances obtained for the wave heights provided by the simulation are in good agreement with the majority of observations and conclusions described by [20]. See [10] for more details. Furthermore, we see that the computed standard deviation on account of the uncertain parameters is about $5 - 10\%$ of the mean. Compared to the initial parameter uncertainty of 30% of mean, we see that the nonlinear evolution has damped the uncertainty and the problem is fairly insensitive or moderately sensitive to the three uncertain parameters. Thus, it enhances our confidence in previously reported numerical simulations of this event [10].

The CUDA implementation of the MLMC-FV-IFCP method has been executed on a Tesla K20. For the case of 39 s. we have obtained a runtime of 3120.0 seconds. The MC-FV-IFCP method has also been executed on the same graphics card with $M = 256$ samples, reaching a runtime of 30671.5 seconds, that is, approximately 10 times slower than the MLMC-FV-IFCP method.

7 Conclusion

Many geophysical flows of interest, such as tsunamis generated by rockslides, avalanches, debris etc are modeled by Coulomb type shallow-water models of granular flows following the pioneering work of Savage-Hutter [28]. These models are characterized by model parameters such as ratio of layer densities, Coulomb friction angle and interlayer friction. The values of these parameters are prone to uncertainty on account of heterogeneous composition of the granular material. Consequently, the task of quantifying the resulting solution uncertainty (UQ) is of paramount importance in these simulations.

In this paper, we have presented a novel UQ paradigm by combining a efficient IFCP numerical scheme that can accurately and robustly discretize the underlying non-conservative hyperbolic system (2.1) together with a novel, Multi-level Monte Carlo statistical sampling algorithm. The algorithm is based on computing on nested sequences of mesh resolutions and estimating statistical quantities by combining results from different resolutions. The method is fully non-intrusive, easy to parallelize, fast and accurate. In particular, one can gain several orders of magnitude in computational efficiency vis a vis the standard Monte Carlo method.

We test the algorithms on a set of numerical examples that include both laboratory scale models as well as the realistic two-dimensional models of the Lituya Bay mega tsunami of 1958. The numerical results clearly indicate that the MLMC-IFCP framework can approximate statistics of quantities of interest such as run-up heights, quite accurately and with reasonable computational cost. There was also qualitative and quantitative agreement with experimental and observed data. Furthermore, the UQ simulations help in identifying the sensitivity of simulation outputs to the underlying uncertain parameters. Thus,

they will enable an effective appraisal of sensitivity and enhance risk analysis and hazard mitigation.

The current paper served to illustrate the power and utility of the MLMC UQ paradigm for one realistic set of geophysical problems. Clearly, given the non-intrusiveness, efficiency and robustness of this method, the paper will hopefully lead to application of this paradigm for quantifying uncertainty in a wide range of problems in geophysics.

References

[1] H. Bijl, D. Lucor, S. Mishra and C. Schwab, Eds, *Uncertainty quantification in computational fluid dynamics*, Springer lecture notes in CSE, LNCSE 92, 2014, Springer verlag.

[2] Bouchut F., Mangeney-Castelnau A., Perthame B. & Vilotte J.P.: A new model of Saint-Venant and Savage-Hutter type for gravity driven shallow water flows, *C. R. Math. Acad. Sci. Paris*, 336 (2003), no.6, 531–536.

[3] M.J. Castro, A.M.Ferreiro, J.A. García, J.M. González, J. Macías, C. Parés, M.E. Vázquez. *On the numerical treatment of wet/dry fronts in shallow flows: applications to one-layer and two-layer systems*. Math. Comp. Model. 42 (3-4): 419-439, 2005.

[4] Castro, M.J., Pardo, A., Parés, C., Toro, E.: On some fast well-balanced first order solvers for nonconservative systems, *Math. Comp.*, DOI: 10.1090/S0025-5718-09-02317-5.

[5] Castro Díaz, Manuel J. and Gallardo, José M. and Parés, Carlos High order finite volume schemes based on reconstruction of states for solving hyperbolic systems with nonconservative products. Applications to shallow-water systems *Math. Comp.*, 255:1103-1134, 2006.

[6] Q.Y. Chen, David Gottlieb and Jan S. Hesthaven Uncertainty analysis for the steady-state flows in a dual throat nozzle *J. of Computat. Phys.* 204 (2005) 378-398.

[7] NVIDIA, NVIDIA Developer Zone, `http://developer.nvidia.com/category/zone/cuda-zone`, Accessed February 2014.

[8] Dal Maso G., Lefloch P. & Murat F., Definition and weak stability of nonconservative products *J. Math. Pures Appl.*, (9) 74 (1995), no. 6, 483–548.

[9] Degond, P., Peyrard, P-F., Russo, G. and Villedieu, Ph.: *Polynomial upwind schemes for hyperbolic systems*, C. R. Acad. Sci. Paris Ser. I, 328 (1999), pp. 479–483.

[10] M. de la Asunción, Manuel J. Castro, José M. González, J. Macías, S. Ortega, and C. Sánchez, Modeling the Lituya Bay landslide-generated mega-tsunami with a Savage-Hutter shallow water coupled model, Technical memorandum, 2013.

[11] M. de la Asunción, José M. Mantas, Manuel J. Castro, and S. Ortega, Scalable simulation of tsunamis generated by submarine landslides on GPU clusters, Parallel Computing, submitted.

[12] Fernánchez, E.D., Bouchut, F., Bresch, D. Castro-Díaz, M.J and Mangeney, A.: A new Savage-Hutter type models for submarine avalanches and generated tsunami. *J. Comput. Phys.*, 227:7720–7754, 2008.

[13] Fernández-Nieto, E.D., Castro, M.J. and Parés, C.: On an Intermediate Field Capturing Riemann Solver Based on a Parabolic Viscosity Matrix for the Two-Layer Shallow Water System. *J. Sci. Comput.* 48, 1-3 (July 2011).

[14] Fritz, D.J. and Hager, W.H. and Minor, H.-E, Lituya Bay case: rockslide impact and wave runup, Science of Tsunami Hazards, 19(1),(3-22),2001

[15] Fritz, H.M. and Mohammed, F. and Yoo, J, Lituya Bay landslide impact generated mega-tsunami 50th anniversary Pure Appl. Geophys., 166(1-2) (153-175), 2009

[16] Giles, M Improved multilevel Monte Carlo convergence using the Milstein scheme. *Preprint NA-06/22, Oxford computing lab, Oxford, U.K*, 2006.

[17] Giles, M Multilevel Monte Carlo path simulation. *Oper. Res.*, 56:607-617, 2008.

[18] Heinrich, S. Multilevel Monte Carlo methods. Large-scale scientific computing. *Third international conference LSSC 2001, Sozopol, Bulgaria. Lecture Notes in Computer Science, Vol 2170, Springer Verlag* (2001), pp. 58-67.

[19] M. Matsumoto, and T. Nishimura, Mersenne twister: a 623-dimensionally equidistributed uniform pseudo-random number generator, ACM Trans. on Modeling and Computer Simulation, 8(1),(3-30),1998

[20] Miller, D.J. Giant Waves in Lituya Bay, Alaska: A Timely Account of the Nature and Possible Causes of Certain Giant Waves, with Eyewitness Reports of Their Destructive Capacity *Professional paper,* 1960.

[21] Mishra, S. and Schwab, C. Sparse tensor multi-level Monte Carlo Finite Volume Methods for hyperbolic conservation laws with random initial data. *Math. Comp.* January, 2011.

[22] Mishra, S., Schwab, C. and Sukys, J. Multi-level Monte Carlo finite volume methods for nonlinear systems of conservation laws in multi-dimension. *J. Comput. Physics.*, 231:3365-3388. April, 2012.

[23] Mishra, S., Schwab, C. and Sukys, J. Multilevel Monte Carlo Finite Volume Methods for Shallow Water Equations with Uncertain Topography in Multi-dimensions. *SIAM J. Scientific Computing.*, 34, 6. 2012

[24] Parés, C., Castro, M.J.: On the well-balance property of Roes method for nonconservative hyperbolic systems. Applications to shallow water systems. *Math. Model. Numer. Anal.* 38(5), 821-852 (2004)

[25] Parés, C.: Numerical methods for nonconservative hyperbolic systems: a theoretical framework. *SIAM J. Numer. Anal.*, 44 (1), 300-321 (2006).

[26] C. Parés and M.L. Muñoz Ruíz. On some difficulties of the numerical approximation of nonconservative hyperbolic systems. *Boletín SEMA*, 47:23-52, 2009.

[27] G. Poette, B. Després and D. Lucor. Uncertainty quantification for systems of conservation laws. *J. Comput. Phys.*, 228:2443-2467, 2009.

[28] S.B. Savage and K. Hutter: The motion of a finite mass of granular material down a rough incline. *J. Fluid Mech.*, 199:177–215, 1989.

[29] S. Tokareva Stochastic finite volume methods for computational uncertainty quantification in hyperbolic conservation laws *Diss., Eidgenossische Technische Hochschule ETH Zurich, Nr. 21498, 2013*

[30] J. Tryoen, O. Le Maitre, M. Ndjinga and A. Ern Intrusive projection methods with upwinding for uncertain non-linera hyperbolic systems *Journal of Computational Physics* 229, 18 (2010) 6485-6511.

[31] Xiu, D. and Hesthaven, J. S. High-order collocation methods for differential equations with random inputs. *SIAM J. Sci. Comput.*, 27, 1118-1139, 2005.

[32] Zabaras, N. and Ma, X. An adaptive hierarchical sparse grid collocation algorithm for the solution of stochastic differential equations. *J. Comp. Phys.*, 228, 3084-3113, 2009.

Acknowledgments

This research has been partially supported by the Spanish Government Research project MTM2012-38383-C02-01, Andalusian Government Research project P11-FQM-8179 and the Swiss Federal Institute of Technology, ETH. (Zurich). The work of SM was partially supported by the ERC STG NN. 306279, SPARCCLE.

Recent Research Reports

Nr.	Authors/Title

2014-14 J. Dick and F.Y. Kuo and Q.T. Le Gia and Ch. Schwab
Multi-level higher order QMC Galerkin discretization for affine parametric operator equations

2014-15 Ch. Schwab
Exponential convergence of simplicial hp-FEM for H ¹-functions with isotropic singularities

2014-16 P. Grohs and S. Keiper and G. Kutyniok and M. Schaefer
α-Molecules

2014-17 A. Hiltebrand and S. Mishra
Efficient computation of all speed flows using an entropy stable shock-capturing space-time discontinuous Galerkin method

2014-18 D. Conus and A. Jentzen and R. Kurniawan
Weak convergence rates of spectral Galerkin approximations for SPDEs with nonlinear diffusion coefficients

2014-19 J. Doelz and H. Harbrecht and Ch. Schwab
Covariance regularity and H-matrix approximation for rough random fields

2014-20 P. Grohs and S. Hosseini
Nonsmooth Trust Region Algorithms for Locally Lipschitz Functions on Riemannian Manifolds

2014-21 P. Grohs and A. Obermeier
Optimal Adaptive Ridgelet Schemes for Linear Transport Equations

2014-22 S. Mishra and Ch. Schwab and J. Sukys
Multi-Level Monte Carlo Finite Volume methods for uncertainty quantification of acoustic wave propagation in random heterogeneous layered medium

2014-23 J. Dick and Q. T. Le Gia and Ch. Schwab
Higher order Quasi Monte Carlo integration for holomorphic, parametric operator equations